



Image guidance for robotic minimally invasive coronary artery bypass

Michael Figl^{a,f,*}, Daniel Rueckert^a, David Hawkes^c, Roberto Casula^d, Mingxing Hu^c, Ose Pedro^a, Dong Ping Zhang^a, Graeme Penney^e, Fernando Bello^b, Philip Edwards^{a,b}

^a Department of Computing, Imperial College London, UK

^b Department of Biosurgery and Surgical Technology, Imperial College London, UK

^c Centre of Medical Image Computing, University College London, UK

^d Cardiothoracic Surgery, St. Mary's Hospital, London, UK

^e Division of Imaging Sciences, King's College London, UK

^f Center for Biomedical Engineering and Physics, Medical University of Vienna, Austria

ARTICLE INFO

Article history:

Received 31 January 2009

Received in revised form 25 July 2009

Accepted 7 August 2009

Keywords:

Image-guided therapy

Registration

Medical robotics

Endoscopic procedures

ABSTRACT

A novel system for image guidance in totally endoscopic coronary artery bypass (TECAB) is presented. Key requirement is the availability of 2D–3D registration techniques that can deal with non-rigid motion and deformation. Image guidance for TECAB is mainly required before the mechanical stabilisation of the heart, when the most dominant source of misregistration is the deformation and non-rigid motion of the heart.

To augment the images in the endoscope of the da Vinci robot, we have to find the transformation from the coordinate system of the preoperative imaging modality to the system of the endoscopic cameras.

In a first step we build a 4D motion model of the beating heart. Intraoperatively we can use the ECG or video processing to determine the phase of the cardiac cycle, as well as the heart and respiratory frequencies. We then take the heart surface from the motion model and register it to the stereo endoscopic images of the da Vinci robot resp. of a validation system using photo-consistency. To take advantage of the fact that there is a whole image sequence available for registration, we use the different phases together to get the registration. We found the similarity function to be much smoother when using more phases. This also showed promising behaviour in convergence tests.

Images of the vessels available in the preoperative coordinate system can then be transformed to the camera system and projected into the calibrated endoscope view using two video mixers with chroma keying. It is hoped that the augmented view can improve the efficiency of TECAB surgery and reduce the conversion rate to more conventional procedures.

© 2009 Elsevier Ltd. All rights reserved.

1. Introduction

1.1. Augmented reality and applications in surgery

Augmented reality (AR) systems applied to surgery aim to overlay additional information, most often in form of images or renderings, onto the real view of the surgeon. Using a stereoscopic device has the potential advantage of enabling 3D perception of both the surgical field and overlays, potentially allowing virtual structures appear beneath the real surface as though the tissue were transparent.

Several AR devices have been developed for applications in medicine. Head mounted displays (HMDs) have been proposed, among others, by Fuchs et al. [1], Birkfellner et al. [2] or Wendt et al. [3].

HMDs generally suffer from fast head movements often causing misregistration. Only few have therefore ever left their laboratories, and most appear in latency or stereo perception measurements, phantom, cadaver or animal studies [4–8].

AR systems using devices that remain in fixed positions, such as operating microscopes [9,10] or undergo tremor reduced movements such as the stereo endoscopes used with the da Vinci robotic operating system are more promising to proceed to the operating theatre.

In this paper we describe a system for image-guided robotic surgical treatment of coronary artery disease. We aim to enhance the endoscopic view provided by the da Vinci robot with information from preoperative imaging.

1.2. Clinical need

Totally endoscopic coronary artery bypass (TECAB) is a minimally invasive robotic cardiac procedure performed on the beating heart. A stereo endoscope gives the surgeon a 3D view of the oper-

* Corresponding author at: Center for Biomedical Engineering and Physics, Medical University of Vienna, Waehringer Guertel 18-20, Austria. Tel.: +431 40400 5471; fax: +431 40400 3988.

E-mail addresses: mfigl@doc.ic.ac.uk, michael.figl@meduniwien.ac.at (M. Figl).

ative field. Surgical tools are driven by intuitive manipulators that provide 7 degrees-of-freedom as well as smoothing and magnification of motion. The endoscope and tools are introduced into the patient through small incisions, minimising the resulting trauma.

TECAB has the potential to treat coronary artery disease without the need for invasive sternotomy or heart–lung bypass. However, there is still a conversion rate to more invasive methods of 20–30% [11–13]. This can occur if there is misidentification of the target vessel or difficulty in locating the artery if it is hidden by fat.

For this reason there has been some interest in introducing image guidance to TECAB. Mourgues and Coste-Maniere [14] and Adhami and Coste-Maniere [15] proposed such a system where the preoperative model comes from bilateral X-rays. Mylonas et al. [16] proposed gaze-contingent tracking to stabilise the motion of the heart and Stoyanov et al. [17] demonstrated soft-tissue tracking based on robust feature tracking.

We have identified two critical points in the procedure that might gain from intraoperative guidance. During harvesting of the left internal mammary artery the position of the bifurcation would be useful to know to allow surgery to progress rapidly to this point. After opening of the pericardium overlay of the target vessel will allow accurate location and identification. It is hoped that such guidance will make surgery more efficient and reduce the conversion rate for TECAB.

Furthermore if excessive pericardial fat can be seen in preoperative scans it usually represents a contra-indication to TECAB because of potential vessel misidentification. Image guidance could enable TECAB to be performed in more difficult cases.

2. Materials and methods

We use a HP xw9400 workstation with two dual output graphics adapters (nVidia Quadro FX 1500) that provide the overlays to each eye, and a four channel frame grabbing device (Active Silicon, Uxbridge, UK) for the purposes of registration. All video images were interlaced with 25 full images per second. The target of our work is the da Vinci robot which is equipped with a stereo endoscope and stereo video output via BNC and S-video.

Overlay on the view through the da Vinci is provided using two video mixers (Panasonic WJ-MX 50) with chroma keying functionality. This ensures that there is no increased lag introduced by the system. The video output of the ECG is also connected to frame grabber. The layout of the system can be seen in Fig. 1, the quality of chroma keyed overlay can be seen in Fig. 2.

As a development and validation system two Sony DCR-TRV 30E digital video cameras were used instead of the da Vinci stereo endoscope. The video cameras were calibrated using a calibration toolbox implemented in MatLAB by Jean-Yves Bouguet [18]. The Sony cameras allowed for a simpler calibration avoiding radial distortion compared to the endoscope.

A further calibration has to be done to register the input coordinates of the video mixer to its output coordinates. This was done by a point to point registration with scaling using the method published in [19].

To achieve guidance a 4D model of the beating heart is required, as the coronary vessels move with the heart movement. This must be both temporally and spatially registered to the patient. Finally the model must be visualised using the calibrated endoscopes.

2.1. 4D model construction

The preoperative model of the patient comes from coronary CT, which provides a fully 4D representation of the patient. The CT can be reconstructed at up to 20 phases throughout the cardiac cycle, see Fig. 3 for an example. The relevant vessels must be segmented

along with the surface of the myocardium. As they are part of the 4D model, their motion will be modelled as well.

We segmented one phase using a semiautomatic region growing method implemented in [20]. We then applied the non-rigid registration method in [21], which is implemented in the software *rview*[20] to propagate this phase to the others, an example of a patient model can be seen in Fig. 7.

2.2. Model-based 2D–3D registration techniques

Having obtained a preoperative model of the patient's heart we now need to align this model to the video view through the da Vinci endoscope.

Our strategy in performing registration is to separate the temporal and spatial alignment of the preoperative model.

Temporal alignment can be obtained using the ECG signal, e.g. via the video output from the ECG which is connected to the frame grabber, see Fig. 1.

Having established temporal registration, the remaining motion will be rigid apart from possible deformation of the heart due to breathing [22].

The main parameters for the 4D motion model, heart rate and respiratory frequency were found by image processing. They were determined using a video sequence of the beating heart and comparing one of the images with all the others using cross-correlation as a similarity measure. The frequencies were then found as peaks in the Fourier transform of this function.

Aligning the phases of the video sequence and the 4D CT is done by visual judgment. There are several time points that can easily be found in both the rendered CT surface and the video sequences and can be used for temporal synchronisation, e.g. the end of the systolic phase, where the heart is in maximal contraction. In practice this could also be achieved using the ECG signal.

To establish correspondence we used photo-consistency [23,24] as a similarity measure applied to the calibrated stereo views that are available on the da Vinci system.

2.3. Photo-consistency

The idea behind registration using photo-consistency is to judge whether given projections of a surface are compatible with the lighting model. Assuming a Lambertian lighting model [25] a surface point should have the same colour in all of its projections.

Fig. 4 gives an example, where three points have similar colour values in different images. The mean standard deviation of a certain colour and a certain point over all three images is 2.3 in an 8 bit colour space, but the standard deviation for the green component in the three points of the second image is 26.2. With a Lambertian light model specular reflections as seen in the lower front of the heart phantom in Fig. 4 cannot be addressed.

For the registration we have to find the rigid body transformation T from the coordinate system of the surface(-model) to the common coordinate system of the camera calibrations. After applying this transformation the surface object will be in a position where the projections of the surface points are (photo-)consistent. This consistency can be evaluated using the colour components of the projections of the surface points x in different video channels i . If the colour diversity in the images is evaluated by their variance, then the desired transformation T can be found by:

$$T = \operatorname{argmin} \left(\operatorname{mean}_x \left(\operatorname{var}_i \left(\operatorname{colour}(P_i T x) \right) \right) \right) \quad (1)$$

where P_i denotes the projection matrix for camera calibration i . Fig. 5 shows the situation for three cameras.

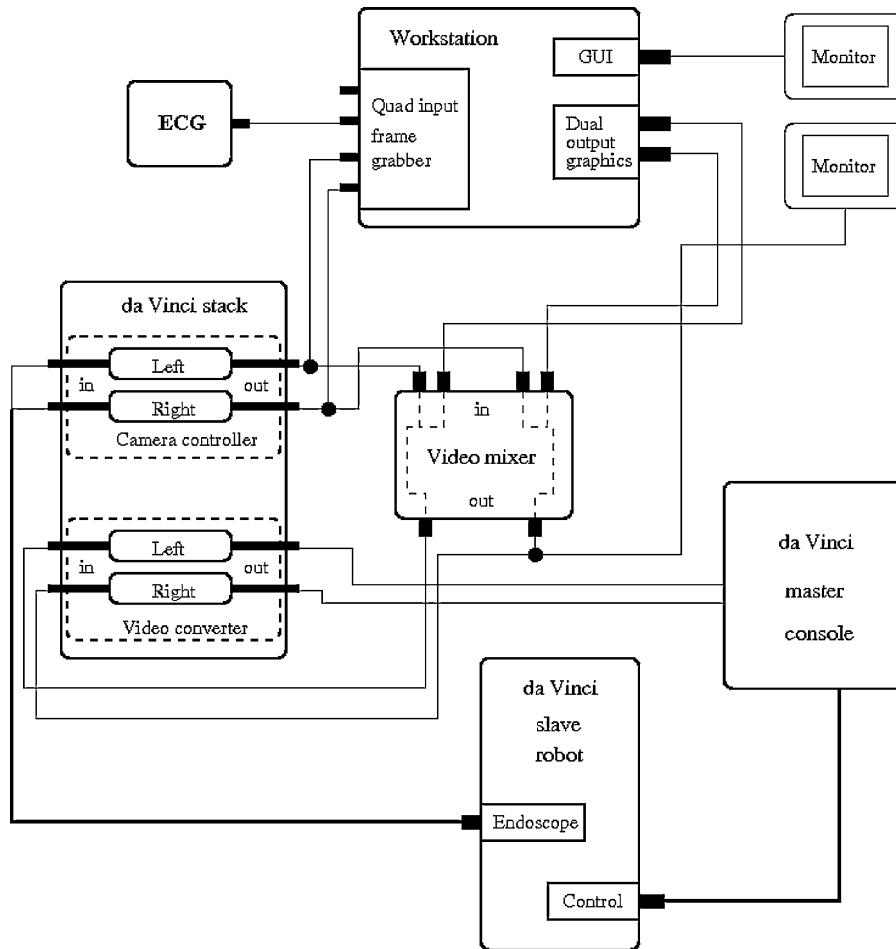


Fig. 1. The layout of the system in theatre. ECG and the stereo video are grabbed by the machine to gain parameters we need for the image overlay, e.g. the heart and breathing frequencies. The resulting images from the dual graphics output are overlaid to the real video images using video mixers. There is no delay of the real video images in the view of the surgeon as they are just copied to our PC (there is a direct connection from the camera controller via the video mixer to the converter and the master console).

Photo-consistency as a similarity measure for 2D–3D registration was introduced by Clarkson et al. [24]. A normalised cost function is presented in order to control outliers:

$$PC_{\text{normalised}} := \text{mean}_x \frac{\varepsilon^2}{\varepsilon^2 + \text{var}_i(\text{colour}(P_iTx))} \quad (2)$$

The damping parameter ε has to be chosen according to the expected noise level in the image [24].

The algorithm was implemented on the HP xw9400 workstation running Fedora Linux in C++ using OpenGL and the `glut` library. To exclude hidden points, e.g. from the backside of the surface, the depth buffer was used.

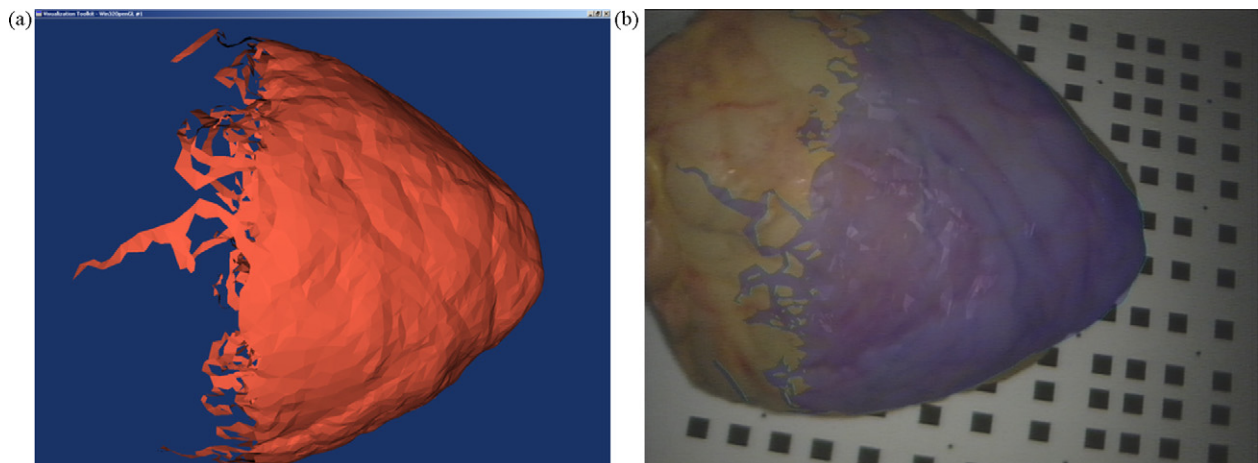


Fig. 2. The surface of a heart phantom and the overlay using chroma keying. (a) shows the rendering of the surface. The surface file is truncated to visualise the difference to the heart phantom underneath as can be seen in (b).

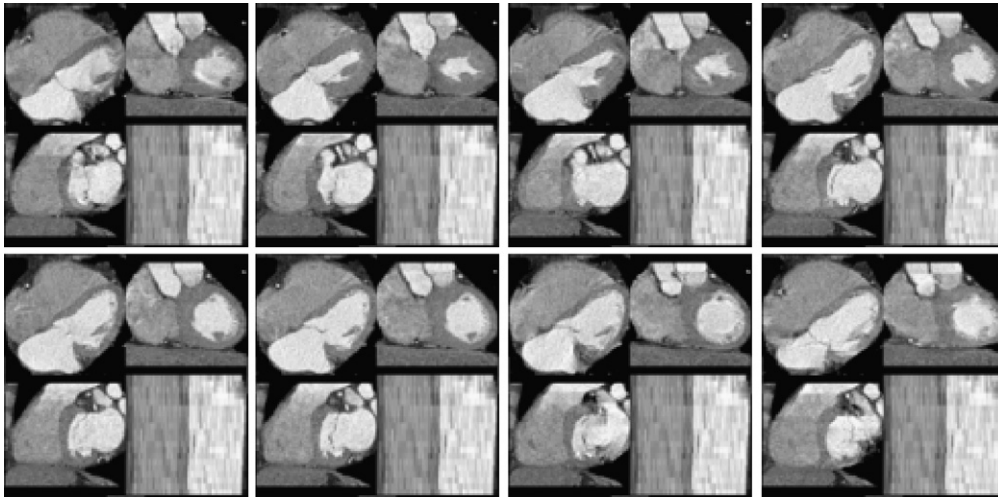


Fig. 3. The phases of a heart displayed using the software `rview`. Only about half of the 20 phases are shown.

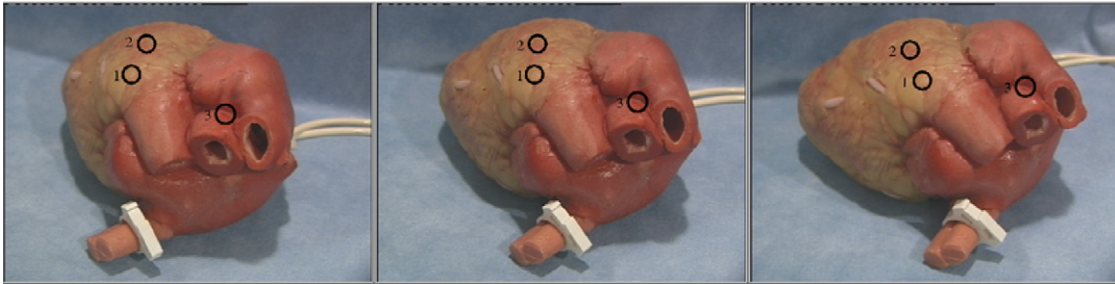


Fig. 4. With Lambert's light model the colours in the centers of the circles 1, 2, and 3 should be the same in every image. The mean standard deviation of colours values in these points is 2.3 in an 8 bit colour space. On the lower front of the second and third image there is a considerable reflection which does not comply with the Lambertian model and has a very different colour in the first image. (For interpretation of the references to colour in this figure legend, the reader is referred to the web version of the article.)

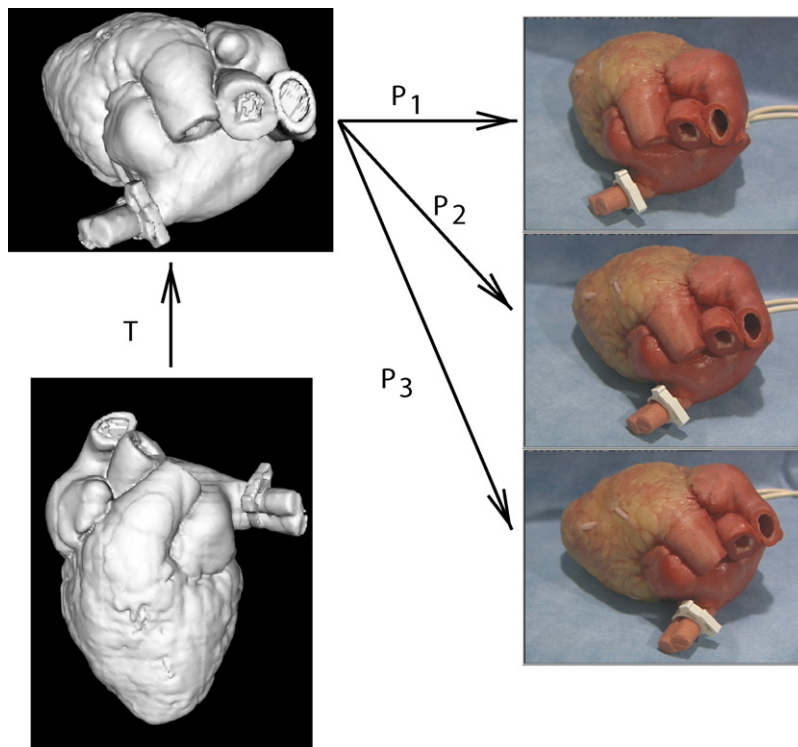


Fig. 5. The transformation T has to move the surface object in a way that the projections of every point of the surface into the video images using the camera calibrations P_i are photo-consistent. In the case of the Lambert light model they have to have the same colour.

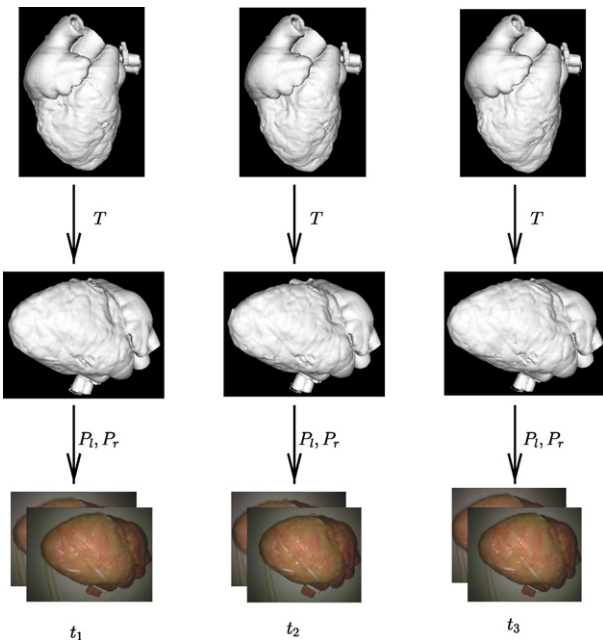


Fig. 6. The transformation between the preoperatively generated surfaces and the intraoperative position is the same for all phases, provided there is no camera movement or respiration.

2.4. Photo-consistency using an image sequence

To take advantage of the fact that there is a whole image sequence available for registration, one can try to use the different phases together to derive the transformation. Assuming that all the deformation or movement of the object can be found in the surfaces and is completely periodic, the transformation from the preoperative to the intraoperative coordinate system is always the same. In Fig. 6 the chain of transformations from the preoperative coordinates system to the display is shown for three different phases. Both the transformation T and the camera calibrations are unchanged in this idealised situation.

Computation of photo-consistency is expensive as it uses all points in the image, therefore a good starting position is needed for the minimisation in Eq. (1). This starting value for the transformation T is found by identification of several corresponding points x_l, x_r in the left and right image and on the surface followed by minimising the distance of the projected surface points to the image points iteratively:

$$T = \operatorname{argmin}_{\text{points}} \sum (||P_l T x - x_l||^2 + ||P_r T x - x_r||^2) \quad (3)$$

2.5. Heart phantom

To test the accuracy and convergence of the registration procedure we used a motion model generated from a 4D CT scan of a pneumatic heart phantom built by the Chamberlain Group, Great Barrington, MA, USA.

The phantom was scanned by a Philips Brilliance 64 ECG triggered CT, and reconstructed at 10 different phases of the cardiac cycle. The ECG signal for the heart phantom was generated by a signal generator from Hameg, Mainhausen, Germany, using the heart rate found by image processing as mentioned in Section 2.2. The surfaces of the 10 phases were extracted using the marching cubes algorithm implemented in VTK (Kitware Inc, NY, USA). The surface had 180,460 triangles. No sub-sampling was done, i.e. the points

were used for registration. We did not construct a 4D model from the heart phantom data set, the surfaces were used as-is.

3. Results

3.1. Camera calibration and video mixer calibration

For camera calibration we used 12 images of a checkerboard pattern with 11×9 squares for every channel. The baselines of the squares was 7.5 mm. Typical calibration errors with the endoscope were 0.51 and 0.45 pixels in x resp. y direction for the separate channels before undistortion and stereo calibration. After undistortion and stereo calibration the distortion coefficients were 10 times smaller and the errors in the same magnitude as before, in a concrete example 0.4 resp. 0.33 pixels.

The input–output calibration for the video mixers had a mean error of 0.6 pixels.

3.2. 4D model construction

For preoperative model building we use coronary CT images reconstructed at 20 even phases throughout the cardiac cycle. To produce a 4D model we segment the first phase by hand and propagate this to the other 19 phases by non-rigid registration using [20]. This is similar to the method used by Wierzbicki et al. [26], but here it is demonstrated on clinical coronary CT scans rather than phantom data. Fig. 7 gives an idea of the quality of the registration.

3.3. Model parameters

Heart and respiratory rate could easily be determined using the method described in Section 2.2, for endoscopic videos of a patient's beating heart and also for image sequences of the heart phantom. Fig. 8a shows the Fourier transform of the cross-correlation. The heart rate measured on the patient was identical to the ECG measured heart rate. The phantom's heart rate could be verified by counting.

3.4. Photo-consistency registration

To evaluate the registration method without introducing errors by the camera calibration, the temporal alignment or the quality of the video images we did a first registration series from the surface model to renderings of the surfaces. The renderings were made using camera calibration data from the robot's stereo endoscope. The normalised photo-consistency function, as defined in formula (2) was used. We found the similarity function to be smoother when more phases were used. To quantify this, the total variation normalised by the range was derived:

$$TV(f) := \frac{1}{\max(f) - \min(f)} \int ||f' || \quad (4)$$

The variations can be found in Table 1a.

Using the development system consisting of two Sony video cameras we did measurements comparable to those done with the renderings.

In this test series absolute photo-consistency as defined in formula (1) and up to 10 phases of the heart cycle were used. In Fig. 9 the situation at the minimum for translation along the z -axis of the world coordinate system is shown when using 1, 5, or 10 phases. The corresponding normalised total variations for the functions in Fig. 9 were 1.69, 1.43, and 1.4. The remaining variations can be found in Table 1b.

Furthermore we made a test series to compare the convergence, starting at 5 different positions. The starting positions were

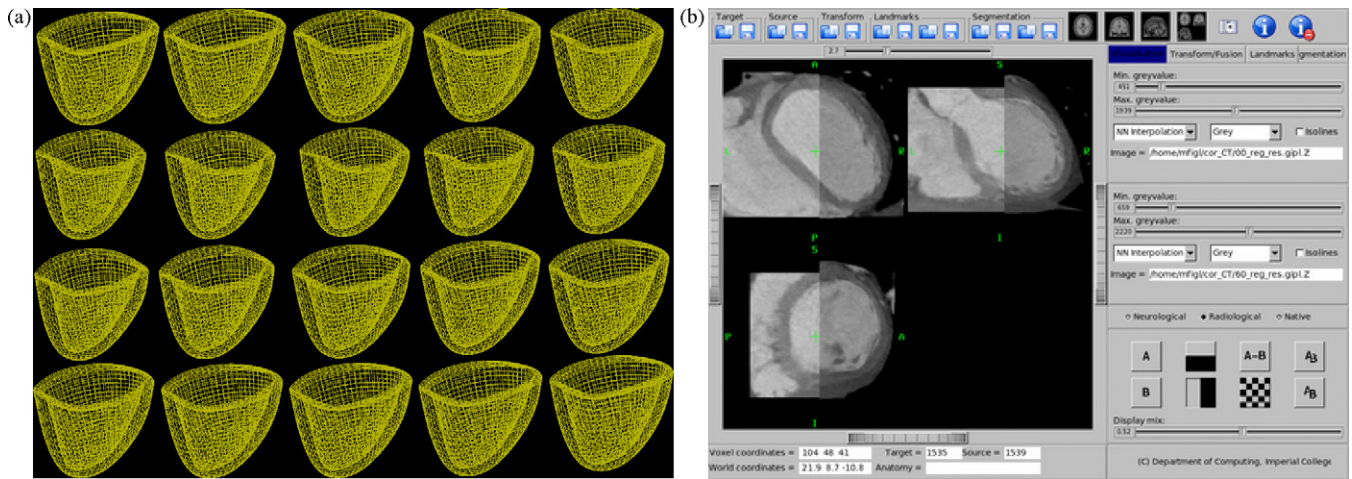


Fig. 7. Non-rigid registration was used to register the first image to the other images. In (a) the deformation of the ventricle is displayed. (b) shows the registered image slices from different phases (0% and 60%) of the cardiac cycle.

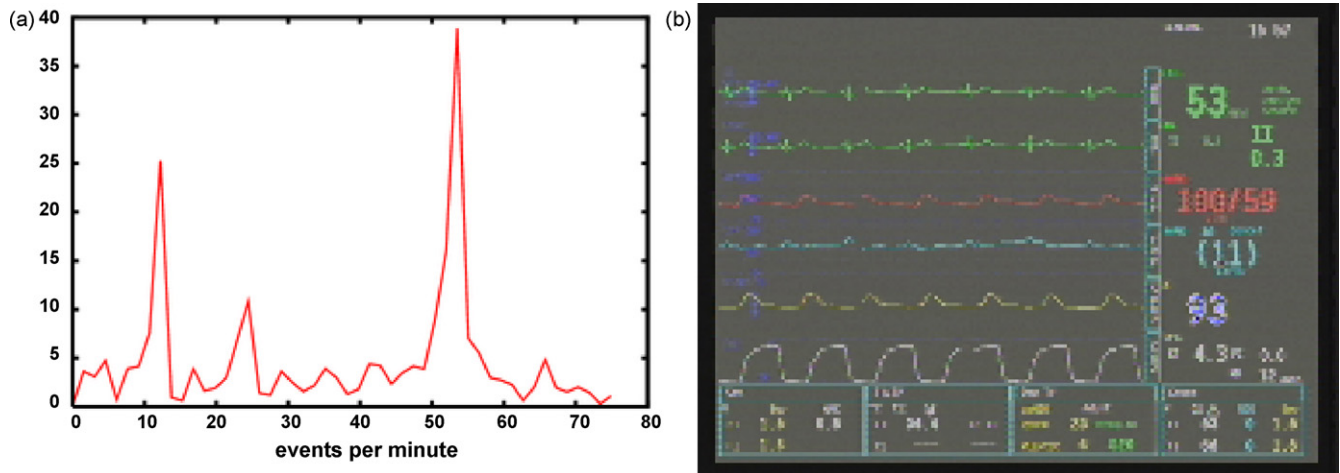


Fig. 8. (a) shows the Fourier transform of the cross-correlation from the image number 12 to the other images of a video sequence of the beating heart like in Fig. 10c. Two main frequencies can be seen 12 and 54 beats per minute, breathing and the heart beat. (b) shows the corresponding ECG display grabbed with the frame grabber.

chosen using a minimum point of the similarity function and then changing this with random numbers. The random numbers were generated using the built in function `int random()`. As they are equally distributed in $[0, \text{RAND_MAX}]$ we did $(\text{value}/\sqrt{6}) \cdot 2 \cdot ((\text{random()}/\text{RAND_MAX}) - 0.5)$ with `value=14` as a target distance. One resp. five phases were used with the normalised photo-consistency version. The distances to the target point can be found in Table 2a.

Table 1
The normalised total variations for parameter and number of phases for the image sequences.

# Phases	t_x	t_y	t_z	r_x	r_y	r_z
(a) Phantom renderings						
1	1.69	2.12	1.57	2.42	2.08	2.22
2	1.66	2.06	1.72	2.33	1.77	2.17
3	1.43	1.96	1.51	1.84	1.9	2.06
4	1.42	1.95	1.65	1.86	1.73	1.91
5	1.4	1.96	1.55	1.97	1.9	2.1
6	1.48	1.93	1.59	1.76	1.82	1.79
(b) Video images						
1	1.98	2.21	2.06	2.07	3.7	2.47
3	1.74	2.05	1.82	1.64	2.9	2.1
5	1.73	1.88	1.82	1.61	2.6	1.96
10	1.64	1.76	1.73	1.48	2.07	1.88

Another test series with the same method but the absolute photo-consistency function, a target `value=20` and changes just in the translation components was done. The results can be found in Table 2b.

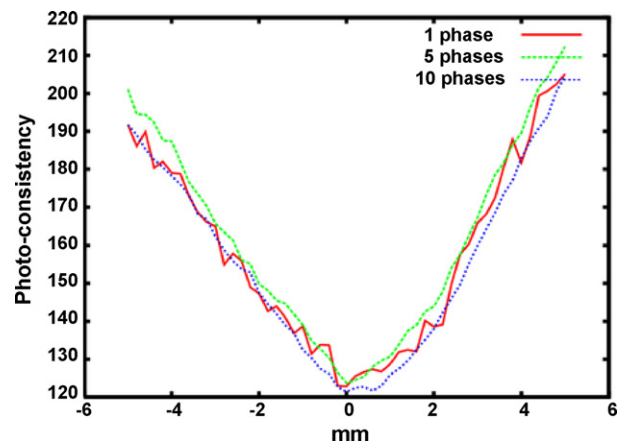


Fig. 9. The image shows translation along the z-axis vs. photo-consistency at the minimum point using 1, 5, and 10 phases for the video sequence. Total variations are 1.69, 1.43, and 1.4, for 1, 5, resp. 10 phases.

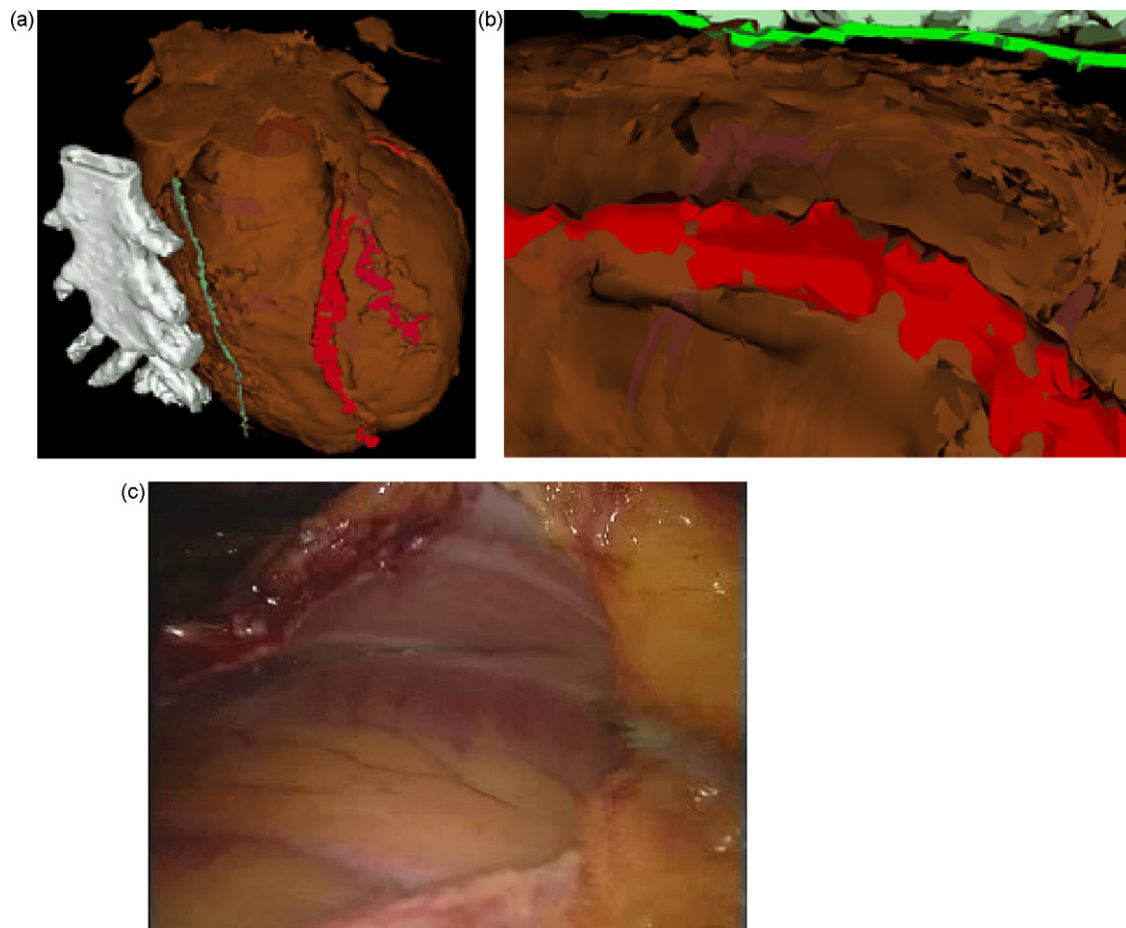


Fig. 10. A rendering of the preoperative model showing the myocardial surface, left internal mammary artery, left anterior descending artery and a diagonal branch (a), an aligned rendering (b) and its corresponding endoscope view (c).

3.5. Visualisation

An example of retrospectively aligned images is shown in Fig. 10. We have a number of clinical coronary CT images that are being used to investigate preoperative model construction. Registration algorithms using both feature tracking and intensity-based techniques are being developed.

4. Discussion and conclusion

We presented a system for augmented reality image guidance of totally endoscopic coronary artery bypass. Previous work has suggested the use of image guidance in TECAB surgery and demonstrated its feasibility on a heart phantom [27]. Falk et al. have demonstrated a system for AR guidance based on multi-planar X-ray angiography [28]. We describe the first such results built on clinical coronary CT scans to provide the 4D patient model using non-rigid registration. Heart and respiratory frequencies as param-

eters needed to adjust the model to the concrete clinical situation were derived using image processing. We aligned the phase by visual judgment but it could also be found in the ECG.

We are also examining whether geometry constraints can be used as an accurate means of finding the period of the heart cycle, in the presence of rigid motion of the camera or near rigid motion due to breathing, a first result has been published in [29]. We also presented a novel strategy for alignment of this model to the endoscopic view, using photo-consistency for registration. From the figures in Table 1a and b we can conclude that the similarity function is smoother in the meaning of the definition in formula (4) when using more phases. More interesting might be the probable consequences for the convergence which are illustrated in Table 2a and b and show promising behaviour for deviations in the translation component but unfortunately not much improvement if the rotation is included. We will investigate whether hierarchical methods could improve the convergence.

Segmentation was done manually in this paper, but additionally we are investigating the use of a 4D statistical model to produce a segmentation [30] and also the use of a subdivision surface representation of the heart with volume preservation to track the motion of the myocardium [31].

An additional complexity in reality is also the heart motion due to breathing [22]. Preliminary work has shown that 3D–3D non-rigid registration can be used to build separate models of respiratory motion of heart [22]. Since both respiratory and cardiac motion are smooth and continuous, 4D parametric motion models based on 4D B-splines could be developed. These motion models could provide compact representations of cardiac motions.

Table 2
Distances to the minimum points for five sequences.

(a) Rotation and translation were changed					
Before	8.5	4.7	7.8	9.3	9.9
One phase	5.8	2.7	6.4	3.8	8.2
Five phases	5.4	2.6	6.4	5.1	7.3
(b) Just the translation components were changed for the starting value					
Before	8.9	11.6	7.6	2.8	9.3
One phase	5.7	3.9	2.4	2.1	4.6
Five phases	4.9	1.0	1.4	1.7	3.5

The confocal light sources for the stereo endoscope of the da Vinci robot were also a difficulty, as they are not compatible with our diffuse light model and cause considerable noise. We could simply ignore the brightest parts of the video images as suggested by Stoyanov et al. [17]. Another potential technique would be to calibrate the position of these light sources and to incorporate specular reflections into our lighting model.

For augmentation of the endoscopic view we use video mixers, which do not introduce any lag to the surgeon's view of the real surface. We use chroma keying for the image fusion, which limits the range of available colours. This is not a significant limitation as we want colour separation between the overlaid view and the largely red surgical view. It is hoped that such information can improve the efficiency of TECAB surgery and reduce the conversion rate to more invasive procedures.

Acknowledgements

We would like to thank the EPSRC for funding this project. We are also grateful to the theatre staff at St Mary's hospital, London and to the radiology staff in St Mary's and the Royal Brompton hospitals for their cooperation. M. Figl was partly supported by FWF project P19931.

References

- [1] Fuchs H, Livingston MA, Raskar R, Colucci D, Keller K, State A, et al. Augmented reality visualization for laparoscopic surgery. In: MICCAI 1998, vol. 1496 of LNCS. Springer; 1998. p. 934–43.
- [2] Birkfellner W, Figl M, Huber K, Watzinger F, Wanschitz F, Hummel J, et al. A head-mounted operating binocular for augmented reality visualization in medicine—design and initial evaluation. *IEEE Trans Med Imaging* 2002;21:991–7.
- [3] Wendt M, Sauer F, Khamene A, Basclé B, Vogt S, Wacker FK. A head-mounted display system for augmented reality: initial evaluation for interventional MRI. *Röfo-Fortschr. Gebiet Röntgenstrahlen Bildgeb Verfahr* 2003;175:418–21.
- [4] Birkfellner W, Figl M, Matula C, Hummel J, Hanel R, Imhof H, et al. Computer enhanced stereoscopic vision in a head-mounted operating binocular. *Phys Med Biol* 2003;48:N49–57.
- [5] Wanschitz F, Birkfellner W, Figl M, Patruta S, Wagner A, Watzinger F, et al. Computer-enhanced stereoscopic vision in a head-mounted display for oral implant surgery. *Clin Oral Implants Res* 2002;13(6):610–6.
- [6] Figl M, Ede C, Hummel J, Wanschitz F, Ewers R, Bergmann H, et al. A fully automated calibration method for an optical seethrough head-mounted operating microscope with variable zoom and focus. *IEEE Trans Med Imaging* 2005;24(11):1492–9.
- [7] Wacker F, Vogt S, Khamene A, Jesberger J, Nour S, Elgort D, et al. An augmented reality system for MR image-guided needle biopsy: initial results in a swine model. *Radiology* 2006;238(2):497–504.
- [8] Das M, Sauer F, Schoepf U, Khamene A, Vogt S, Schaller S, et al. Augmented reality visualization for ct-guided interventions: system description, feasibility, and initial evaluation in an abdominal phantom. *Radiology* 2006;240(1):230–5.
- [9] Edwards PJ, King AP, Maurer Jr CR, de Cunha DA, Hawkes DJ, Hill DLG, et al. Design and evaluation of a system for microscope-assisted guided interventions (MAGI). *IEEE Trans Med Imaging* 2000;19(11):1082–93.
- [10] Edwards PJ, Johnson LG, Hawkes DJ, Fenlon MR, Strong AJ, Gleeson MJ. Clinical experience and perception in stereo augmented reality surgical navigation. In: MIAR vol. 3150 of LNCS. Springer; 2004. p. 369–76.
- [11] Kappert U, Cichon R, Schneider J, Gulielmos V, Ahmadzade T, Nicolai J, et al. Technique of closed chest coronary artery surgery on the beating heart. *Eur J Cardio-Thorac Surg* 2001;20:765–9.
- [12] Dogan S, Aybek T, Andressen E, Byhahn C, Mierdl S, Westphal K, et al. Totally endoscopic coronary artery bypass grafting on cardiopulmonary bypass with robotically enhanced telemanipulation: report of forty-five cases. *J Thorac Cardiovasc Surg* 2002;123:1125–31.
- [13] Falk V, Diegeler A, Walther T, Banusch J, Brucerius J, Raumans J, et al. Total endoscopic computer enhanced coronary artery bypass grafting. *Eur J Cardio-Thorac Surg* 2000;17:38–45.
- [14] Mourgues F, Coste-Maniere E. Flexible calibration of actuated stereoscopic endoscope for overlay in robot assisted surgery. In: MICCAI, 2002, vol. 2488 of LNCS. Springer; 2002. p. 25–34.
- [15] Adhami L, Coste-Maniere E. A versatile system for computer integrated minimally-invasive robotic surgery. In: MICCAI, 2002, vol. 2488 of LNCS. Springer; 2002. p. 272–81.
- [16] Mylonas GP, Stoyanov D, Deligianni F, Darzi A, Yang GZ. Gaze-contingent soft tissue deformation tracking for minimally invasive robotic surgery. In: MICCAI, 2005, vol. 3749 of LNCS. Springer; 2005. p. 843–50.
- [17] Stoyanov D, Mylonas GP, Deligianni F, Darzi A, Yang GZ. Softtissue motion tracking and structure estimation for robotic assisted mis procedures. In: MICCAI, 2005, vol. 3750 of LNCS. Springer; 2005. p. 139–46.
- [18] J. Bouguet. Camera calibration toolbox for matlab; 2007. Website, available at <http://www.vision.caltech.edu/bouguetj>.
- [19] Horn BKP. Closed form solution of absolute orientation using unit quaternions. *J Opt Soc Am A* 1987;4:629–42.
- [20] D. Rueckert. Image registration toolkit; 2008. Website, available at <http://www.doc.ic.ac.uk/~dr/software/>.
- [21] Rueckert D, Sonoda LI, Hayes C, Hill DLG, Leach MO, Hawkes DJ. Nonrigid registration using free-form deformations: Application to breast MR images. *IEEE Trans Med Imaging* 1999;18(8):712–21.
- [22] McLeish K, Hill DLG, Atkinson D, Blackall JM, Razavi R. A study of the motion and deformation of the heart due to respiration. *IEEE Trans Med Imaging* 2002;21:1142–50.
- [23] Clarkson MJ, Rueckert D, Hill DLG, Hawkes DJ. A multiple 2D video-3D medical image registration algorithm. In: Proc. SPIE Medical Imaging 2000, vol. 3979. 2000. p. 342–52.
- [24] Clarkson MJ, Rueckert D, Hill DLG, Hawkes DJ. Using photoconsistency to register 2D optical images of the human face to a 3D surface model. *IEEE Trans Pattern Anal Mach Intell* 2001;23:1266–80.
- [25] Foley JD, van Dam A, Feiner SK, Hughes JF. Computer graphics. 2nd ed. Addison Wesley; 1995.
- [26] Wierzbicki M, Drangova G, Guiraudon G, Peters T. Validation of dynamic heart models obtained using non-linear registration for virtual reality training, planning, and guidance of minimally invasive cardiac surgeries. *Med Image Anal* 2004;8:387–401.
- [27] Szpala S, Wierzbicki M, Guiraudon G, Peters T. Real-time fusion of endoscopic views with dynamic 3-D cardiac images: a phantom study. *IEEE Trans Med Imaging* 2005;24(9):1207–15.
- [28] Falk V, Mourgues F, Adhami L, Jacobs S, Thiele H, Nitzsche S, et al. Cardio navigation: planning, simulation, and augmented reality in robotic assisted endoscopic bypass grafting. *Ann Thorac Surg* 2005;79:2040–8.
- [29] Hu M, Penney G, Rueckert D, Edwards P, Figl M, Pratt P, et al. A novel algorithm for heart motion analysis based on geometric constraints. In: MICCAI, 2008, vol. 5241 of LNCS. Springer; 2008. p. 720–8.
- [30] Perperidis D, Mohiaddin R, Edwards P, Rueckert D, Hill, Segmentation of cardiac MR and CT image sequences using model-based registration of a 4D statistical model. In: Proc. SPIE Medical Imaging 2007, vol. 6512. 2007.
- [31] Chandrashekar R, Mohiaddin R, Razavi R, Rueckert R. Nonrigid image registration with subdivision lattices: application to cardiac MR image analysis. In: MICCAI 2007, vol. 4791 of LNCS. Springer; 2007. p. 335–42.